Applied Physics Letters

Simultaneously enhanced electrical conductivity and suppressed thermal conductivity for ALD ZnO films via purge-time controlled defects

Cite as: Appl. Phys. Lett. **120**, 062106 (2022); https://doi.org/10.1063/5.0081657
Submitted: 09 December 2021 • Accepted: 30 January 2022 • Published Online: 10 February 2022

Ramin Ghiyasi, Milena Milich, John Tomko, et al.

Applied Physics Letters ARTICLE scitation.org/journal/apl

Simultaneously enhanced electrical conductivity and suppressed thermal conductivity for ALD ZnO films via purge-time controlled defects

Cite as: Appl. Phys. Lett. **120**, 062106 (2022); doi: 10.1063/5.0081657
Submitted: 9 December 2021 · Accepted: 30 January 2022 ·
Published Online: 10 February 2022

Ramin Ghiyasi,[1] Milena Milich,[2] John Tomko,[2] Girish C. Tewari,[1] Mika Lastusaari,[3] Patrick E. Hopkins,[2] and Maarit Karppinen[1,a)]

AFFILIATIONS

[1]Department of Chemistry and Materials Science, Aalto University, FI-00076 Espoo, Finland
[2]University of Virginia, Department of Mechanical and Aerospace Engineering, Charlottesville, Virginia 22904, USA
[3]Department of Chemistry, University of Turku, FI-20014 Turku, Finland

[a)]Author to whom correspondence should be addressed: maarit.karppinen@aalto.fi

ABSTRACT

We demonstrate the simultaneous manipulation of electrical and thermal transport characteristics of ZnO thin films fabricated via the prototype atomic layer deposition (ALD) process from diethyl zinc (DEZ) and water precursors. The key ALD process parameter is the length of the N_2 purge applied after the DEZ precursor pulse. We characterize the thin films with x-ray reflectivity measurements for the film growth characteristics, with photoluminescence spectroscopy for structural defects, with electrical transport measurements for carrier density, electrical resistivity, and Seebeck coefficient, and with time-domain thermoreflectance measurements for thermal conductivity. Photoluminescence spectroscopy data suggest that elongation of the purge period creates structural defects, which increase the electron carrier density; this would explain the enhanced electrical conductivity of the films. At the same time, the defects are likely to hinder the thermal transport in the films. The, thus, realized simultaneous increase in electrical conductivity and decrease in thermal conductivity are of fundamental importance in thermoelectrics. Moreover, the simple control of the intrinsic electrical transport properties is highly desired for the semiconducting ZnO films in optics and microelectronics.

Thermoelectric energy harvesters are increasingly investigated for new application areas;[1] a strongly emerging application area is seen in wearable electronics, which could be powered by flexible thermoelectric thin-film body heat harvesters.[2–4] The heat to electricity conversion capability of thermoelectric materials is evaluated by the figure-of-merit, $ZT = S^2\sigma T/\kappa$, which can be maximized by increasing the Seebeck coefficient (S) and electrical conductivity (σ) and decreasing the thermal conductivity ($\kappa = \kappa_e + \kappa_{ph}$) at the operation temperature (T). Here, the challenge is that increasing the carrier density (n) to increase σ is bound to increase the electronic part of thermal conductivity (κ_e). This underlines the importance of manipulating the phononic part of thermal conductivity (κ_{ph}) through, e.g., lattice defects or nanostructuring, that is, using strategies independent of the carrier concentration.[5]

The phonon contribution is especially large for metal oxides, such as ZnO. Zinc oxide is a wide-bandgap semiconductor and is transparent to visible light, and as a simple, nontoxic, and critical-element-free compound, it is highly attractive for future industrial applications,[6–11] including the thermoelectrics,[12–15] transparent conductors,[16,17] biosensors,[18] and solar cells.[19] For all these applications, high-quality thin films with tailorable transport properties are needed. Atomic layer deposition (ALD) thin-film technology is compatible with most of the requirements posed by these applications.[7,20–22] It is based on reactive gaseous precursors sequentially pulsed and purged in and out of the reactor to induce self-saturated surface reactions, thereby allowing precise film thickness control, large-area homogeneity, and high-aspect-ratio conformality for the produced thin films and coatings. Moreover, ALD is compatible with sensitive substrates, such as polymers,[4,9] and uniquely integrable with textiles as it has been shown to conformally coat the textile fibers in such a way that the whole textile may become part of the device; this is especially beneficial considering the aforementioned wearable thermoelectric applications.[4,23]

Fabrication of ZnO thin films from diethyl zinc (DEZ) and water precursors is one of the prototype ALD processes.[7] Also, the literature

includes a variety of ways to control the electrical and thermal transport properties of these films, through elemental substitutions,[22,24,25] intercalation of organic layers,[12,15,26,27] precursor,[28–30] and process parameter optimization,[28,31–38] as well as post-deposition processing.[39] Among the process parameters, very little has been paid attention to the purge time optimization,[28,31,40] as the inert gas (typically N_2) purge period between the two precursor pulses is often just arbitrary chosen to be long enough for the complete removal of the excessive precursor and reaction by-product molecules from the reactor lines and chamber. However, there are few previous studies indicating possible effects of the purge time and its flow rate[41] on the film growth rate[31] and electrical properties[28,40] of ALD ZnO thin films. In the present letter, we will systematically elucidate the effects of the purge time after the DEZ precursor pulse, first on the film growth characteristics and then on the basic properties of the resultant ZnO films (smoothness, density, defects). Most excitingly, we will demonstrate how this simple process parameter can be used to simultaneously enhance electrical conductivity and suppress thermal conductivity.

We deposited a series of ZnO films from diethyl zinc (>95%, Strem Chem.) and de-ionized water (H_2O) using a commercial ALD reactor (Picosun R-100); the film depositions were carried out simultaneously on silicon (Okmetic Oyj; $2 \times 2\,cm^2$), borosilicate glass (Finnish Special Glass Oy; $2 \times 1\,cm^2$), and sapphire (MTI corp.; $1 \times 1\,cm^2$) substrates to enable the x-ray diffraction (XRD), x-ray reflectivity (XRR; Panalytical XPert diffractometer; Cu-K_α), photoluminescence (PL; Lotis TII Nd:YAG laser at 355 nm with Avantes HS-TEC CCD detector), electrical transport (Physical Property Measurement System; PPMS; Quantum Design; 9T magnet; standard four point-probe technique), and thermal transport (time-domain thermoreflectance or TDTR method) characterization; experimental details of the characterizations are given in the supplementary material. Both precursors were kept at room temperature, and N_2 gas (99.999%; Parker nitrogen generator: HPN2-5000C-L-230V) was utilized as both the purge and carrier gas with a precisely regulated flow rate of 150 sccm. All depositions were carried out exactly at 220 °C with an excessive one-hour stabilization time before the actual precursor pulsing to avoid even the smallest possible thermal fluctuations during the depositions. Unless otherwise stated, the precursor pulsing sequence was: 0.1 s DEZ/varied N_2/0.2 s H_2O/0.4 s N_2. The total number of these ALD cycles was fixed to 600 to keep the precursor intake exactly the same for all the depositions.

All the thin-film samples deposited were confirmed by XRD to be polycrystalline wurtzite-structured ZnO films with no visible deposition parameter-dependent changes in orientation preference; a representative XRD pattern is shown in the supplementary material. In our initial tests, we varied the N_2 purge length (after the DEZ pulse) in the relatively wide range from 0.1 to 2.0 s and analyzed carefully the XRR patterns of the resultant ZnO films for their thickness, roughness, and density; the fitting protocol is described in detail in the supplementary material; and the results are summarized in Fig. 1. It was revealed that the film thickness (expressed as GPC: growth-per-cycle) and roughness values monotonously decrease with the increasing purge length, while for the film density, a very weak increasing trend from 5.26 to 5.39 g/cm^3 could be seen. Similar observations have been previously reported for ALD ZnO films and explained by an etching effect of the purge gas on the surface zinc atoms and/or hydroxyl groups.[28,31,40,41] Indeed, since the etching effect is likely to be strongest from the

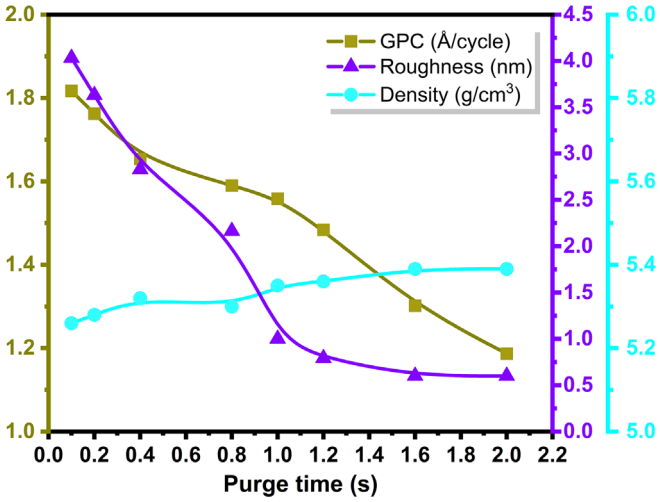

FIG. 1. Growth characteristics based on XRR data for ZnO films deposited with different N_2 purge times: GPC (left), film roughness (right), and density (rightmost).

so-called surface hills, it is easy to understand that the partial surface group removal makes the surface smoother during the film growth, as noticed here. For the rest of the investigations, we decided on a set of five ZnO thin-film samples grown with the purge lengths of 0.1, 0.2, 0.4, 0.8, and 1.2 s; these films were deposited simultaneously on different substrate types needed for the different characterizations.

Photoluminescence spectroscopy has been widely applied for the characterization of various defects in ZnO thin films. We carried out PL measurements for the three samples with purge periods of 0.1, 0.2, and 1.2 s; the spectra are shown in Fig. 2. The room-temperature bandgap emission peak for various ZnO nanostructures is reported to appear in the range from 377 to 397 nm;[42] for all our samples, this intense peak is seen around 394 ± 2 nm. Then, the possible defects in ZnO (oxygen and zinc vacancies and interstitials) should be seen as

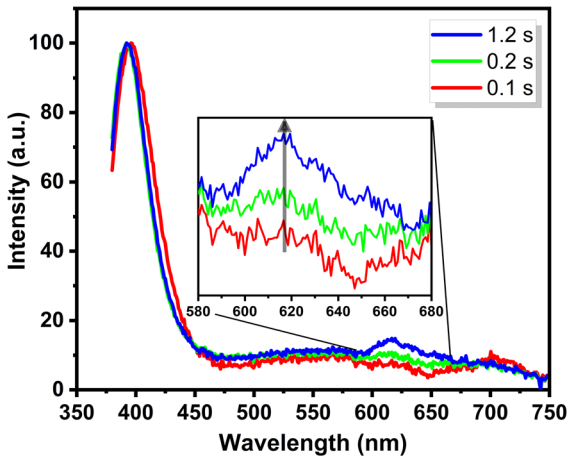

FIG. 2. Photoluminescence spectra for ZnO films deposited with different purge times of 0.1, 0.2, and 1.2 s (normalized to total intensity).

weaker peaks at the higher wavelengths,[39,42–44] and in general, the higher bandgap emission peak intensity compared to the higher-wavelength defect peak intensities indicates a high-quality film structure,[45] as is also the case for the present samples. A variety of different defects with peaks at different wavelengths have been reported for ZnO.[42,46,47] In the 450–750 nm region measured here, the following defects, if present, should be visible: V_{Zn}^{-}, O_{Zn}, O_i^{-}, $V_O Zn_i$, and V_O^{+}.[42,46,48,49] For the present samples, the only visible defect peak in this range is seen around 619 nm (2.00 eV), which can be assigned to interstitial-type negatively charged oxygen defects (O_i^{-}).[43,50,51] Since the intensity of this 2-eV peak increases for our ZnO films with the increasing purge time, it seems that the surface etching effect (presumably removing part of the latest-deposited Zn atoms from the surface) might simultaneously create O_i^{-} centers inside the film, as illustrated in Fig. 3. Recently, Li *et al.*[52] suggested that such negatively charged oxygen centers would form tetrahedral interstitial sites, where the negative charge of oxygen is actually balanced by three partially positive hydrogen atoms. Most importantly, these defects were found to increase the n-type doping of ZnO, explained by transitions from shallow donors (hydrogen) to deep acceptors (oxygen) in the tetrahedral interstitial site.[52,53]

The electronic transport property data (temperature dependence of charge carrier density, electrical resistivity, and Seebeck coefficient) for four samples (with purge periods of 0.2, 0.4, 0.8, and 1.2 s) are presented in Fig. 4. The Hall coefficient was found to be negative for all the samples implying electrons as the primary charge carriers. For each sample, the charge carrier density either decreases slightly or roughly remains the same with the decreasing temperature, see the top panel in Fig. 4. Electrical resistivity for the samples shows semiconducting behavior increasing with the decreasing temperature. Comparison within the sample series shows that the carrier density increases strongly with the increasing purge period, tentatively interpreted here to be due to the electron doping through the higher O_i^{-} defect concentration. Accordingly, the resistivity decreases in the same order for the samples. For example, the room-temperature charge carrier density is an order of magnitude higher and resistivity is two orders of magnitude lower for the 1.2-s sample compared to the 0.2-s sample. We note that the decreased surface roughness seen for the samples with the increasing purge period (Fig. 1) could also contribute to the reduction in electrical resistivity. In accordance with the Hall measurement data, the Seebeck coefficient is negative for all the samples and decreases (in magnitude) with the increasing purge period as presented in the bottom panel of Fig. 4. Considering the dependence, $|S| \approx \sqrt{\rho}/n^{2/3}$, both the increase in charge carrier density and the decrease in electrical resistivity contribute to this trend.

The electronic part of thermal conductivity can be estimated from the electrical resistivity using the Wiedemann–Franz Law, $\kappa_e = LT/\rho$, where L is Lorentz number ($2.44 \times 10^{-8}\ W\,\Omega\,K^{-2}$). At 300 K, the κ_e value increases on the order of 0.003, 0.01, 0.03, and $0.1\ W\,m^{-1}\,K^{-1}$ with the increasing purge period from 0.2 to 1.2 s. All these values are negligibly small, though, underlining the fact that the thermal conductivity of our ZnO films is dominated by phonons, and thus, the effect of the increase in electron carrier concentration on thermal conductivity is minimal.

The thermal conductivity values measured at 300 K for the three ZnO thin films (and the associated interfaces) with purge periods of 0.1, 0.4, and 1.2 s are presented in Table I. From these data, the overall κ value decreases with the increasing purge period, that is, in a way opposite to the κ_e value, indicating that also κ_{ph} decreases with the increasing purge period. This could be explained by the suggested formation of the tetrahedral defect sites (besides the charge carriers) during the elongated purge periods; these defects cause phonon scattering and result in the observed reduction in thermal conductivity.[54]

The thermal conductivity measurements were conducted using the time-domain thermoreflectance method; see the supplementary material for the measurement details. In addition to a trend in thermal conductivity, we also observed an interesting trend in thermal boundary conductance. Due to the strong decrease in surface roughness with

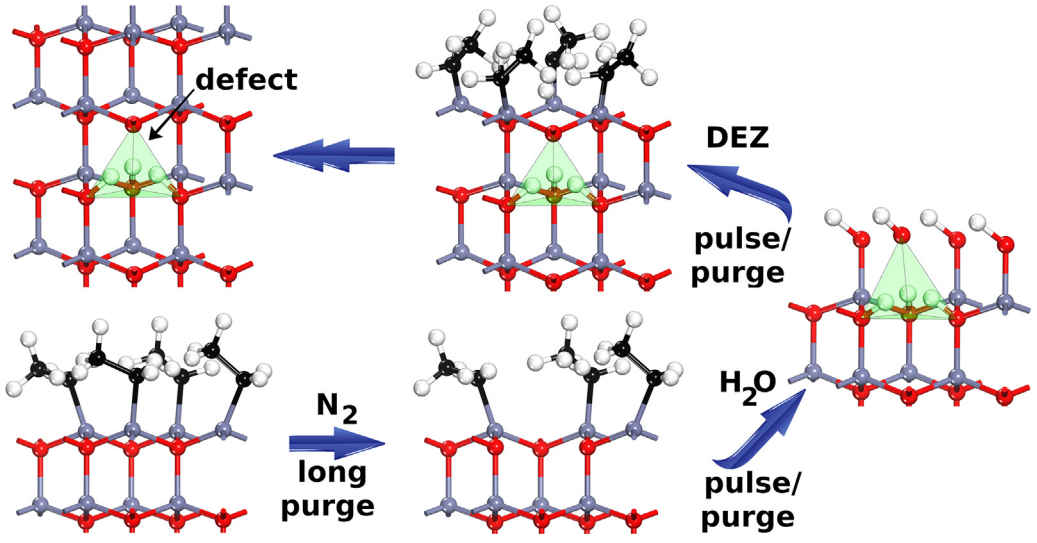

FIG. 3. Schematic representation of the defect formation mechanism tentatively suggested to explain the transport properties (color code: red: oxygen, white: hydrogen, gray: zinc, and black: carbon).

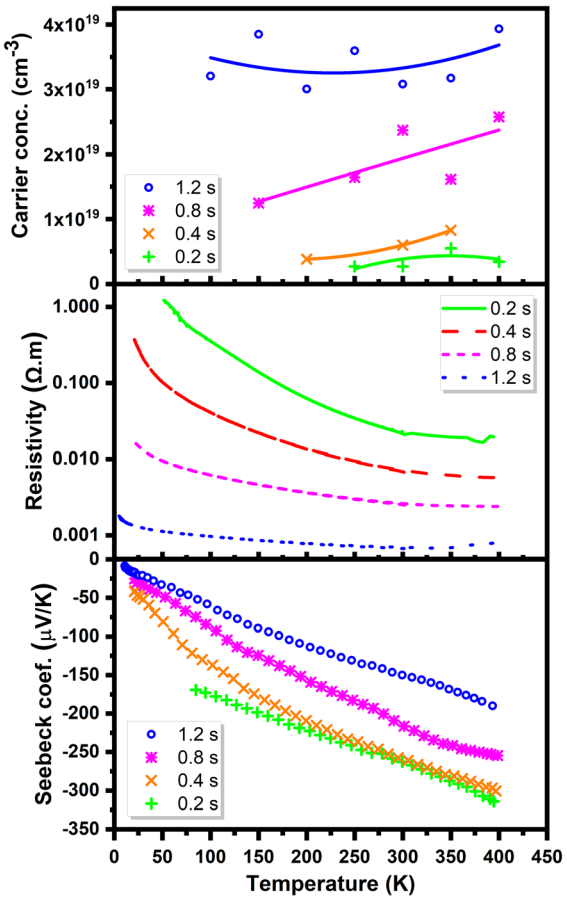

FIG. 4. Temperature dependence of electrical transport properties for ZnO films deposited with different purge times (0.2, 0.4, 0.8, and 1.2 s): carrier concentration (n), resistivity (ρ), and Seebeck coefficient (S).

the longer purge periods, we expected to see a corresponding decrease in resistance at the transducer (Al):ZnO interface. We instead see the opposite trend. By then examining the thermoreflectance signal in the early times after the ultra-fast heating pulse, we observe strong effects of acoustic mismatch due to the large difference in elastic modulus between Al and ZnO. The large jump in material hardness at the interface causes a portion of the pulse energy to be simply reflected from the interface and returned to the sample surface rather than transmitted to ZnO. The slightly higher density ZnO films that correspond to longer purge times result in a larger percentage of energy to be reflected from the interface, and thus, a lowered measured thermal boundary conductance. This experimentally observed trend is in agreement with the trend in transmission coefficient as calculated using the acoustic mismatch model. Thus, in addition to the observed decrease in thermal conductivity with the longer purge periods, we also observe a change in mechanical properties between the films.

TABLE I. Thermal conductivity values for ZnO films deposited with different purge times (0.1, 0.4, and 1.2 s) and associated interfaces.

Purge time (s)	Effective thermal conductivity ($W\ m^{-1}\ K^{-1}$)	Transmission coefficient	Secondary peak amplitude (%)
0.1	7.71	0.92	0.55
0.4	7.53	0.92	1.57
1.2	7.00	0.92	2.66

In conclusion, our work demonstrates that by controlling the conventional ALD growth process for ZnO thin films with a single deposition process parameter only, that is, the length of the N_2 purge after the diethyl zinc precursor pulse, it is possible to systematically control the electrical and thermal conductivity properties of the films. These changes in transport properties were tentatively explained as follows: by lengthening the purge period, a small etching effect is achieved, which removes some Zn atoms from the surface and accordingly creates n-type defects within the growing film. This makes the films smoother, as the Zn atoms are preferably removed from the "hilly" parts of the growth surface. Importantly, the electron carrier density and, accordingly, the electrical conductivity are found to increase as well. The most attractive result is that despite the increased carrier density, the thermal conductivity of the films was found to decrease. This was attributed to the positive effect of the formed defects, which were assumed to serve as a source of phonon blocking, enabling the simultaneously enhanced electrical conductivity and suppressed thermal conductivity. Our results are highly valuable considering the possible thermoelectric applications. Moreover, the possibility to tailor the intrinsic electrical conductivity of ALD ZnO thin films is most important for many other applications as well.

See the supplementary material for a detailed description of the measurement procedures.

The authors acknowledge the extensive use of the RawMatters Finland Infrastructure (RAMI) at Aalto University. Funding was received from the European Union's Horizon 2020 research and innovation programme under the Marie Skłodowska-Curie Grant Agreement (No. 765378), and also from Academy of Finland (Profi-3, PREIN) and the Army Research Office (No. W911NF-16-1-0406).

AUTHOR DECLARATIONS

Conflict of Interest

The authors have no conflicts to disclose.

DATA AVAILABILITY

The data that support the findings of this study are available from the corresponding author upon reasonable request.

REFERENCES

[1]L. Yang, Z.-G. Chen, M. S. Dargusch, and J. Zou, "High performance thermoelectric materials: Progress and their applications," Adv. Energy Mater. **8**, 1701797 (2018).
[2]Y. Wang, L. Yang, X.-L. Shi, X. Shi, L. Chen, M. S. Dargusch, J. Zou, and Z.-G. Chen, "Flexible thermoelectric materials and generators: Challenges and innovations," Adv. Mater. **31**, 1807916 (2019).
[3]Y. Du, J. Xu, B. Paul, and P. Eklund, "Flexible thermoelectric materials and devices," Appl. Mater. Today **12**, 366 (2018).

[4]G. Marin, R. Funahashi, and M. Karppinen, "Textile-integrated ZnO-based thermoelectric device using atomic layer deposition," Adv. Eng. Mater. **22**, 2000535 (2020).
[5]*Thermoelectrics Handbook*, edited by D. M. Rowe (Routledge, London, England, 2018).
[6]Ü. Özgür, Y. I. Alivov, C. Liu, A. Teke, M. A. Reshchikov, S. Doğan, V. Avrutin, S.-J. Cho, and H. Morkoç, "A comprehensive review of ZnO materials and devices," J. Appl. Phys. **98**, 041301 (2005).
[7]T. Tynell and M. Karppinen, "Atomic layer deposition of ZnO: A review," Semicond. Sci. Technol. **29**, 043001 (2014).
[8]J. Theerthagiri, S. Salla, R. A. Senthil, P. Nithyadharseni, A. Madankumar, P. Arunachalam, T. Maiyalagan, and H.-S. Kim, "A review on ZnO nanostructured materials: Energy, environmental and biological applications," Nanotechnology **30**, 392001 (2019).
[9]M. Vähä-Nissi, M. Pitkänen, E. Salo, E. Kenttä, A. Tanskanen, T. Sajavaara, M. Putkonen, J. Sievänen, A. Sneck, M. Rättö, M. Karppinen, and A. Harlin, "Antibacterial and barrier properties of oriented polymer films with ZnO thin films applied with atomic layer deposition at low temperatures," Thin Solid Films **562**, 331–337 (2014).
[10]J. Cembrero, "Nanocolumnar ZnO films for photovoltaic applications," Thin Solid Films **451–452**, 198–202 (2004).
[11]W.-Y. Chang, Y.-C. Lai, T.-B. Wu, S.-F. Wang, F. Chen, and M.-J. Tsai, "Unipolar resistive switching characteristics of ZnO thin films for nonvolatile memory applications," Appl. Phys. Lett. **92**, 022110 (2008).
[12]R. Ghiyasi, M. Milich, J. Tomko, P. E. Hopkins, and M. Karppinen, "Organic-component dependent thermal conductivity reduction in ALD/MLD grown ZnO:organic superlattice thin films," Appl. Phys. Lett. **118**, 211903 (2021).
[13]S. Saini, P. Mele, T. Oyake, J. Shiomi, J.-P. Niemelä, M. Karppinen, K. Miyazaki, C. Li, T. Kawaharamura, A. Ichinose, and L. Molina-Luna, "Porosity-tuned thermal conductivity in thermoelectric Al-doped ZnO thin films grown by mist-chemical vapor deposition," Thin Solid Films **685**, 180–185 (2019).
[14]J.-P. Niemelä, A. J. Karttunen, and M. Karppinen, "Inorganic–organic superlattice thin films for thermoelectrics," J. Mater. Chem. **3**, 10349–10361 (2015).
[15]F. Krahl, A. Giri, J. A. Tomko, T. Tynell, P. E. Hopkins, and M. Karppinen, "Thermal conductivity reduction at inorganic-organic interfaces: From regular superlattices to irregular gradient layer sequences," Adv. Mater. Interfaces **5**, 1701692 (2018).
[16]S. Faÿ, J. Steinhauser, N. Oliveira, E. Vallat-Sauvain, and C. Ballif, "Opto-electronic properties of rough LP-CVD ZnO:B for use as TCO in thin-film silicon solar cells," Thin Solid Films **515**, 8558–8561 (2007).
[17]X.-T. Hao, L.-W. Tan, K.-S. Ong, and F. Zhu, "High-performance low-temperature transparent conducting aluminum-doped ZnO thin films and applications," J. Cryst. Growth **287**, 44–47 (2006).
[18]N. P. Shetti, S. D. Bukkitgar, K. R. Reddy, C. V. Reddy, and T. M. Aminabhavi, "ZnO-based nanostructured electrodes for electrochemical sensors and biosensors in biomedical applications," Biosens. Bioelectron. **141**, 111417 (2019).
[19]K. Djessas, I. Bouchama, J. L. Gauffier, and Z. B. Ayadi, "Effects of indium concentration on the properties of In-doped ZnO films: Applications to silicon wafer solar cells," Thin Solid Films **555**, 28–32 (2014).
[20]S. M. George, "Atomic layer deposition: An overview," Chem. Rev. **110**, 111–131 (2010).
[21]E. Riyanto, E. Martides, E. Junianto, and B. Prawara, "The growth mechanisms of atomic layer deposition: An overview," Eksergi **17**, 56 (2020).
[22]Z. Gao and P. Banerjee, "Review article: Atomic layer deposition of doped ZnO films," J. Vac. Sci. Technol. A **37**, 050802 (2019).
[23]A. J. Karttunen, L. Sarnes, R. Townsend, J. Mikkonen, and M. Karppinen, "Flexible thermoelectric ZnO–organic superlattices on cotton textile substrates by ALD/MLD," Adv. Electron. Mater. **3**, 1600459 (2017).
[24]M. Ohtaki, K. Araki, and K. Yamamoto, "High thermoelectric performance of dually doped ZnO ceramics," J. Electron. Mater. **38**, 1234–1238 (2009).
[25]L. Han, N. Van Nong, W. Zhang, L. T. Hung, T. Holgate, K. Tashiro, M. Ohtaki, N. Pryds, and S. Linderoth, "Effects of morphology on the thermoelectric properties of Al-doped ZnO," RSC Adv. **4**, 12353 (2014).
[26]T. Tynell, A. Giri, J. Gaskins, P. E. Hopkins, P. Mele, K. Miyazaki, and M. Karppinen, "Efficiently suppressed thermal conductivity in ZnO thin films via periodic introduction of organic layers," J. Mater. Chem. A **2**, 12150–12152 (2014).
[27]R. Ghiyasi, G. C. Tewari, and M. Karppinen, "Organic-component dependent crystal orientation and electrical transport properties in ALD/MLD grown ZnO–organic superlattices," J. Phys. Chem. C **124**, 13765–13770 (2020).
[28]H. Beh, D. Hiller, and M. Zacharias, "Optimization of ALD-ZnO thin films toward higher conductivity," Phys. Status Solidi A **215**, 1700880 (2018).
[29]A. Seweryn, R. Pietruszka, B. S. Witkowski, A. Wierzbicka, R. Jakiela, P. Sybilski, and M. Godlewski, "Structural and electrical parameters of ZnO thin films grown by ALD with either water or ozone as oxygen precursors," Crystals **9**, 554 (2019).
[30]T. Nguyen, N. Adjeroud, M. Guennou, J. Guillot, Y. Fleming, A.-M. Papon, D. Arl, K. Menguelti, R. Joly, N. Gambacorti, and J. Polesel-Maris, "Controlling electrical and optical properties of zinc oxide thin films grown by thermal atomic layer deposition with oxygen gas," Results Mater. **6**, 100088 (2020).
[31]A. Wójcik, M. Godlewski, E. Guziewicz, R. Minikayev, and W. Paszkowicz, "Controlling of preferential growth mode of ZnO thin films grown by atomic layer deposition," J. Cryst. Growth **310**, 284–289 (2008).
[32]J. W. Elam, Z. A. Sechrist, and S. M. George, "ZnO/Al_2O_3 nanolaminates fabricated by atomic layer deposition: Growth and surface roughness measurements," Thin Solid Films **414**, 43–55 (2002).
[33]J. Zhang, H. Yang, Q.-L. Zhang, S. Dong, and J. K. Luo, "Structural, optical, electrical and resistive switching properties of ZnO thin films deposited by thermal and plasma-enhanced Atomic layer deposition," Appl. Surf. Sci. **282**, 390–395 (2013).
[34]E. Guziewicz, M. Godlewski, L. Wachnicki, T. A. Krajewski, G. Luka, S. Gieraltowska, R. Jakiela, A. Stonert, W. Lisowski, M. Krawczyk, J. W. Sobczak, and A. Jablonski, "ALD grown zinc oxide with controllable electrical properties," Semicond. Sci. Technol. **27**, 074011 (2012).
[35]J. Panigrahi, P. K. Singh, G. Gupta, and Vandana, "Growth and luminescence characteristics of zinc oxide thin films deposited by ALD technique," J. Lumin. **233**, 117797 (2021).
[36]E. Guziewicz, M. Godlewski, T. A. Krajewski, Ł. Wachnicki, G. Łuka, W. Paszkowicz, J. Z. Domagała, E. Przeździecka, E. Łusakowska, and B. S. Witkowski, "ZnO by ALD—Advantages of the material grown at low temperature," Acta Phys. Pol., A **116**, 814–817 (2009).
[37]E. Guziewicz, T. A. Krajewski, E. Przezdziecka, K. P. Korona, N. Czechowski, L. Klopotowski, and P. Terziyska, "Zinc oxide grown by atomic layer deposition: From heavily n-type to p-type material," Phys. Status Solidi B **257**, 1900472 (2020).
[38]E. Przeździecka, Ł. Wachnicki, W. Paszkowicz, E. Łusakowska, T. Krajewski, G. Łuka, E. Guziewicz, and M. Godlewski, "Photoluminescence, electrical and structural properties of ZnO films, grown by ALD at low temperature," Semicond. Sci. Technol. **24**, 105014 (2009).
[39]M.-J. Zhao, Z.-T. Sun, Z.-X. Zhang, X.-P. Geng, W.-Y. Wu, S.-Y. Lien, and W.-Z. Zhu, "Suppression of oxygen vacancy defects in sALD-ZnO films annealed in different conditions," Mater. **13**, 3910 (2020).
[40]H. K. Park, B. S. Yang, S. Park, M. S. Kim, J. C. Shin, and J. Heo, "Purge-time-dependent growth of ZnO thin films by atomic layer deposition," J. Alloys Compd. **605**, 124–130 (2014).
[41]J. S. Jur and G. N. Parsons, "Atomic layer deposition of Al_2O_3 and ZnO at atmospheric pressure in a flow tube reactor," ACS Appl. Mater. Interfaces **3**, 299–308 (2011).
[42]A. B. Djurišić and Y. H. Leung, "Optical properties of ZnO nanostructures," Small **2**, 944–961 (2006).
[43]X. L. Wu, G. G. Siu, C. L. Fu, and H. C. Ong, "Photoluminescence and cathodoluminescence studies of stoichiometric and oxygen-deficient ZnO films," Appl. Phys. Lett. **78**, 2285–2287 (2001).
[44]M. Liu, A. H. Kitai, and P. Mascher, "Point defects and luminescence centres in zinc oxide and zinc oxide doped with manganese," J. Lumin. **54**, 35–42 (1992).
[45]H. Ju Ko, Y. Chen, S. Ku Hong, and T. Yao, "MBE growth of high-quality ZnO films on epi-GaN," J. Cryst. Growth **209**, 816–821 (2000).
[46]M. A. Reshchikov, H. Morkoç, B. Nemeth, J. Nause, J. Xie, B. Hertog, and A. Osinsky, "Luminescence properties of defects in ZnO," Physica B **401–402**, 358–361 (2007).
[47]S. A. M. Lima, F. A. Sigoli, M. Jafelicci, Jr., and M. R. Davolos, "Luminescent properties and lattice defects correlation on zinc oxide," Int. J. Inorg. Mater. **3**, 749–754 (2001).
[48]B. Lin, Z. Fu, and Y. Jia, "Green luminescent center in undoped zinc oxide films deposited on silicon substrates," Appl. Phys. Lett. **79**, 943–945 (2001).

[49]P. S. Xu, Y. M. Sun, C. S. Shi, F. Q. Xu, and H. B. Pan, "The electronic structure and spectral properties of ZnO and its defects," Nucl. Instrum. Methods Phys. Res., Sect. B **199**, 286–290 (2003).
[50]X. Liu, X. Wu, H. Cao, and R. P. H. Chang, "Growth mechanism and properties of ZnO nanorods synthesized by plasma-enhanced chemical vapor deposition," J. Appl. Phys. **95**, 3141–3147 (2004).
[51]S. A. Studenikin, N. Golego, and M. Cocivera, "Fabrication of green and orange photoluminescent, undoped ZnO films using spray pyrolysis," J. Appl. Phys. **84**, 2287–2294 (1998).
[52]T. Li, M. Wang, X. Liu, M. Jin, and F. Huang, "Hydrogen impurities in ZnO: Shallow donors in ZnO semiconductors and active sites for hydrogenation of carbon species," J. Phys. Chem. Lett. **11**, 2402–2407 (2020).
[53]M. A. Reshchikov, J. Garbus, G. Lopez, M. Ruchala, B. Nemeth, and J. Nause, "Acceptors in ZnO studied by photoluminescence," in *Materials Research Society Symposia Proceedings* (2006), Vol. 957.
[54]E. A. Scott, "Phonon scattering effects from point and extended defects on thermal conductivity studied via ion irradiation of crystals with self-impurities," Phys. Rev. Mater. **2**, 095001 (2018).